Fine tuning the ionic liquid-vacuum outer atomic surface using ion mixtures

Supplementary Information

Ignacio J. Villar-Garcia[1], Sarah Fearn[1], Nur L. Ismail[2], Alastair J. S. McIntosh[2],
Kevin R. J. Lovelock*[2]

[1] Department of Materials, Imperial College London.
[2] Department of Chemistry, Imperial College London.

Email: kevin.lovelock@imperial.ac.uk
Address: Department of Chemistry
Imperial College London
Exhibition Road, South Kensington
SW7 2AZ
Tel: +44 (0)20 7594 5868

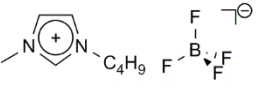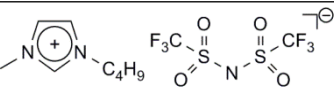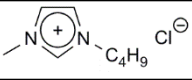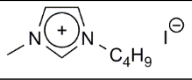### 1. Ionic liquids studied in this paper and synthesis
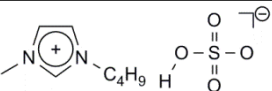
Abbreviation	Structure	Name
$[C_4C_1Im][BF_4]$		1-butyl-3-methylimidazolium tetrafluoroborate
$[C_4C_1Im][Tf_2N]$		1-butyl-3-methylimidazolium *bis*[(trifluoromethane)sulfonyl]imide
$[C_4C_1Im]Cl$		1-butyl-3-methylimidazolium chloride
$[C_4C_1Im]I$		1-butyl-3-methylimidazolium iodide
$[C_4C_1Im][HOSO_3]$		1-butyl-3-methylimidazolium hydrogensulfate

Table S1. Ionic liquids investigated in this work.

The structures of the ionic liquids investigated in this study are shown in Table S1. These ionic liquids were either purchased from: Sigma-Aldrich ($[C_4C_1Im][BF_4]$ and $[C_4C_1Im]I$), or prepared in our laboratory *via* established synthetic methods: $[C_4C_1Im][Tf_2N]$,[1] $[C_4C_1Im]Cl$,[2] or *via* modified procedures ($[C_4C_1Im][HOSO_3]$). The purity of all ionic liquid samples synthesised in our laboratories was assessed using ^{1}H NMR, ^{13}C NMR spectroscopy, and electrospray ionisation and fast atom bombardment mass spectrometry.

<u>Synthesis of 1-butyl-3-methylimidazolium hydrogensulfate [C$_4$C$_1$im][HOSO$_3$]:</u>[3]

60 g of [C$_4$C$_1$im][MeSO$_4$] (240 mmol) were mixed with 10 mL of distilled H$_2$O in a three-necked round bottom flask. 3-4 drops of H$_2$SO$_4$ were added drop-wise to the solution. The solution was stirred at 165 °C in an open round bottom flask to facilitate the removal of boiling methanol from the solution. The flask was also fitted with a dropping funnel containing distilled water and a thermometer. The solution temperature was monitored and maintained at 165 °C by adding the H$_2$O drop-wise into the solution. The progress of the reaction was monitored by the disappearance of the methyl peak in ^{1}H NMR spectrum. After reaction completion the product was dried under vacuum at 50 °C.

^{1}H-NMR (400 MHz, DMSO-d6) δ: 9.93 (1H, s, <u>H</u>SO$_4$), 9.21 (1H, s, NC<u>H</u>N), 7.82 (1H, t, CH$_3$NCHC<u>H</u>N), 7.75 (1H,t, CH$_3$NC<u>H</u>CHN), 4.18 (2H, t, NC<u>H$_2$</u>(CH$_2$)$_2$CH$_3$), 3.87 (3H, s, N-C<u>H$_3$</u>), 1.75 (2H, m, NCH$_2$C<u>H$_2$</u>CH$_2$CH$_3$), 1.20 (2H, m, N-(CH$_2$)$_2$-C<u>H$_2$</u>CH$_3$) and 0.87 (3H, t, N-(CH$_2$)$_3$-C<u>H$_3$</u>). ^{13}C-NMR (400 MHz, DMSO-d_6) δ: 137.18 (N2<u>C</u>H), 123.98 (N<u>C</u>H), 122.74 (N<u>C</u>H), 48.84 (N<u>C</u>H$_2$(CH$_2$)$_2$CH$_3$), 36.06 (N<u>C</u>H$_3$), 31.88 (N-CH$_2$<u>C</u>H$_2$CH$_2$CH$_3$), 19.16 (N(CH$_2$)$_2$<u>C</u>H$_2$CH$_3$) and 13.64 (N(CH$_2$)$_3$<u>C</u>H$_3$). v(neat)/cm-1 3156 - 3101 (aromatic C-H stretch, m), 2963 (aliphatic C-H stretch, m), 1576 (arom. ring def., m), 1161 (asym. S=O stretch, s) 1021 (sym. S=O stretch, s). m/z (LSIMS$^+$) 139 (100%, [C$_4$C$_1$im]$^+$), m/z (LSIMS$^-$) 97 (100%, [HOSO$_3$]$^-$).

2. Low-energy ion scattering (LEIS) apparatus

The ionic samples were introduced into the LEIS chamber load lock and pumped to ~10^{-4} mbar at room temperature for ~16 hours on average. The samples were then introduced into the main LEIS chamber and analysed. LEIS experiments were performed in a Qtac 100 instrument (ION-TOF GmbH) at a base pressure of ~3×10^{-10} mbar (which increases to the 10^{-8} mbar range during the analysis due to the flux of helium gas). We believe the combination of long pump down times, excellent chamber pressures, and the thin films used will add up to removal of all volatile impurities, *e.g.* water. The instrument is fitted with a double toroidal energy analyser (DTA) which collects the scattered ions at a scattering angle of 145° from all azimuth angles. This large solid angle of acceptance combined with parallel energy detection improves the efficiency of the detector by several orders of magnitude in comparison to conventional LEIS instruments and allows the acquisition of higher quality spectra for the same He$^+$ doses. This is especially useful when static conditions are required, *i.e.* the analysis of the sample before significant surface damage occurs. The samples were analysed using a He$^+$ primary ion beam directed perpendicularly to the target surface at 3000 ± 5 eV energy with an analyser pass energy of 3000 eV. Low-energy sputtering was performed by 1 keV Ar$^+$ bombardment at an angle of 59°. In the Supplementary Information, we demonstrate that our LEIS results are representative of the undamaged ionic liquid surface, *i.e.* we operate under static conditions. In addition, the experimental reproducibility, the lack of surface charging, and the sample purity of all of our analysed LEIS samples are also demonstrated. Surface purity was routinely checked before recording LEIS spectra, and if any unexpected peaks were observed, Ar$^+$ bombardment was carried out.

3. Low-energy ion scattering (LEIS) element identification

Element identification was achieved by identifying the presence of characteristic surface peaks. LEIS is an element specific technique. The He$^+$-sample atom interaction can be modelled as a two-body

collision between two quasi-free particles and using the laws of classical mechanics, the energy of the scattered He^{+} can be easily calculated (Equation S1 and Table S2). If an element was present at the sample outer atomic surface in significant concentration a Gaussian-shaped peak was observed at a characteristic energy that is commonly labelled as the surface peak. Table S2 gives the predicted and recorded peak energies, and Table S2 gives the peak energies determined using a peak fitting procedure outlined here in the Supplementary Information.

Based upon the laws of classical mechanics, the following Equation can be determined:

$$\frac{E_F}{E_0} = \left(\frac{(m_2^2 - m_1^2 \cdot \sin^2\theta)^{\frac{1}{2}} + m_1 \cdot \cos\theta}{m_2 + m_1} \right)^2$$

(1)

where E_0 is the kinetic energy of incoming ion, E_F is the kinetic energy of scattered ion, θ is the scattering angle, m_1 is the atomic mass of the incident ion (in our case, for He^{+}) and m_2 is the atomic mass of the scattering (target) atom in the sample.[4, 5] If an element is present at the outer surface in significant concentration a Gaussian-shaped peak is observed at a characteristic energy that can be predicted using Equation 1 (commonly labelled as the surface peak for that element). Table S2 gives the predicted and recorded peak energies. However, due to the He^{+}-target atom collision not being entirely elastic, the observed and predicted energies do not match exactly, *i.e.* the energy observed for a surface peak is always at lower energy than energy predicted.[4, 5]

Element	Molar mass / g mol^{-1}	E_F(predicted) from Equation S1 / eV	E_F(measured) / eV
B	10.8	726	Not detected
C	12.0	848	786 to 819
N	14.0	1028	987 to 1003
O	16.0	1183	1135 to 1143
F	19.0	1377	1326 to 1330
S	32.1	1901	1788 to 1835
Cl	35.5	1986	1897 to 1904
I	126.9	2675	2573

Table S2. E_F(predicted) and E_F(measured) for He^{+} (4 g mol^{-1}) at θ = 145° and E_0 = 3 keV.

4. How a sub-surface peak/tail produced

A peak due to collisions with sub-surface sulfur atoms is produced when: (i) a He^{+} ion penetrates beyond the outer atomic surface of the liquid, (ii) the He^{+} ion collides with a sulfur atom, leading to energy loss and neutralisation to form neutral He[0], (iii) He[0] is re-ionised to form He^{+} (most probably by interaction with an oxygen atom[4]), and (iv) He^{+} is emitted from the liquid towards the analyser. For $[C_4C_1Im]I_{1-x}[Tf_2N]_x$ where $x([Tf_2N]^-) \neq 1$ a characteristic tail due to scattering of He^{+} from sub-surface iodine atoms was observed from ~1900 eV to ~2450 eV (Figure 1a). The intensity of the tail signal changed as $x([Tf_2N]^-)$ was varied: the tail intensity was a maximum at $x([Tf_2N]^-)$ = 0.1, but much lower for $x([Tf_2N]^-)$ = 0. There are two possible explanations for these observations: the amount of sub-surface iodine varies, or the tail intensity is due to both the amount of sub-surface iodine atoms

and also fluorine atoms. We expect that for $[C_4C_1Im]I$ there are sub-surface iodine atoms present, which does not explain the relatively small tail observed for $[C_4C_1Im]I$. Therefore, we ascribe these observations to the presence of fluorine atoms in the mixture, which increased the probability of reionisation of He^0, leading to a larger intensity tail for $x([Tf_2N]^-) = 0.1$ than for $x([Tf_2N]^-) = 0$. For all $[C_4C_1Im][HOSO_3]_{1-x}[BF_4]_x$ mixtures studied a characteristic tail due to scattering of He^+ from sub-surface sulfur atoms was observed from ~1400 eV to ~1750 eV (Figure 2a).

5. Low-energy ion scattering (LEIS) element quantification

An aim of LEIS studies is to determine the outer atomic surface concentration of each element i, N_i. The scattered ion yield for each element in each LEIS spectrum, Y_i, was determined using a peak fitting procedure outlined in the Supplementary Information. S_i is related to N_i by:

$$Y_i = N_i \cdot P_i^+ \cdot d\sigma_i/d\Omega \cdot A \tag{1}$$

where P_i^+ is the ion fraction (the probability that incoming He^+ ions are scattered towards the detector as He^+ ions rather than as neutralised He^0), $d\sigma_i/d\Omega$ is the differential cross-section of the atom probed, and A is a constant based upon experimental variables (see Equation S2 for full details). P_i^+ and $d\sigma_i/d\Omega$ are not known for the elements present in ionic liquids, and determining P_i^+ and $d\sigma_i/d\Omega$ is not trivial; historically it has been achieved by analysis of very pure samples of known surface composition.[5] As determination of N_i is not possible (at least at present), comparison of N_i for different elements is certainly not feasible (at present), e.g. $N_{nitrogen}$ and N_{sulfur} cannot be compared directly from our LEIS results. However, information on N_i can still be gained. P_i^+ and $d\sigma_i/d\Omega$ are expected to depend upon the electronic environment of the target atom. For ionic liquids, the elements present can be in relatively different electronic environments (e.g. sulfur in $[Tf_2N]^-$ and $[SCN]^-$), so it cannot be assumed that P_i^+ and $d\sigma_i/d\Omega$ are constant for each element. However, we assume that P_i^+ and $d\sigma_i/d\Omega$ are constant for an element when it has the same intramolecular bonding, as the electronic environment of this element is expected to be the same. For the nitrogen atoms of the imidazolium ring, it has been demonstrated using XPS and calculations that the atomic charge is dependent upon the anion, but that the atomic charges are still relatively similar.[6] Therefore, in this paper we restrict ourselves to making Y_i comparisons only between elements which have the same intramolecular bonding. This allows us to determine the relative outer atomic surface concentration for an element with particular intramolecular bonding. For example, we can compare Y_{sulfur} for $[cation][Tf_2N]$ ionic liquids, but we do not compare Y_{sulfur} for $[C_4C_1Im][Tf_2N]$ and $[C_4C_1Im][SCN]$; we can compare $Y_{nitrogen}$ for $[C_nC_1Im]^+$ for different ionic liquids.

The measured surface peak area of an element is related to the amount of that element present at the outer atomic surface by:

$$Y_i = N_i \cdot P_i^+ \cdot d\sigma_i/d\Omega \cdot \frac{I_p}{e} \cdot t \cdot \xi \cdot R = N_i \cdot P_i^+ \cdot d\sigma_i/d\Omega \cdot A \tag{2}$$

where Y_i is the scattered ion yield (from a surface atom with mass m_2), N_i is the atomic surface concentration, P_i^+ is the ion fraction (the probability that He particles scattered towards the detector

will be ionised as He^+), $d\sigma_i/d\Omega$ is the differential cross-section (element specific), I_p is the primary ion beam current, e is the elementary charge, t is the acquisition time, ξ is an instrumental factor, R is the correction factor for rough surfaces (R = 1 for a flat surface), and A is a constant for our experimental set-up. Y_i is measured, so to determine N_i the unknowns are P_i^+ and $d\sigma_i/d\Omega$.

6. Low-energy ion scattering (LEIS) detection limit

If a peak due to an element is not observed at the ionic liquid-vacuum outer atomic surface using LEIS it is because N_i for atom i is below our detection limit. The detection limit is determined by two factors: $d\sigma_i/d\Omega$ (and possibly P_i^+ too), and the signal-to-noise ratio for the peak (due to a large background scattered ion yield, see Supplementary Information for more details). In Table S3 approximate detection limits taken from the literature are given for the elements investigated in this study.[5] These values can be used as a qualitative guide to the amount of an element present at the sample outer atomic surface. For example, if a peak is detected for nitrogen, it can be assumed that ≥1% of the ionic liquid-vacuum outer atomic surface is composed of nitrogen atoms.

Elements	Detection limit
Li to O	≥1%
F to Cl	1% to 0.05%

Table S3. Approximate detection limits in atomic percent taken from the literature for the elements investigated in this study.[5]

7. Low-energy ion scattering (LEIS): defining the ionic liquid-vacuum outer atomic surface

How one defines which atoms are in contact with the vacuum is important; the probe used (and its properties) is vital to this definition. For example, the ionic liquid-vacuum outer atomic surface will be different if a relatively large probe such as Br_2 is used compared to when a relatively small He^+ ion probe is used. For $[C_2C_1Im][NO_3]$, hyperthermal $O(^3P)$ atoms were found to penetrate the ionic liquid-vacuum surface about 0.2 nm deeper than for hyperthermal Ar, most likely as the O atom has a smaller van der Waals radius than Ar by ~20%.[7] For LEIS, the He^+ ion probe has a radius of ~0.093 nm,[8] although this estimate is based upon general considerations of ionic radii. Atomic and small molecular probes have also been used.[9-15] Two groups have used intrinsic analysis MD simulations to investigate the composition of the ionic liquid-vacuum outer atomic surface; a probe with a radius of 0.2 nm was used, chosen to be close to the characteristic size of the atoms constituting the system.[16-20]

8. Peak fitting

In this paper we use IONTOF SurfaceLab6 LEIS data evaluation program in order to fit the LEIS spectra and determine peak energies and peak areas. The region due to each element is fitted separately, as demonstrated in our previous paper.[21] In particular, we have detailed previously how to fit the C, O, F and S regions for [cation][Tf_2N].[21]

For the iodine region, we first fitted $[C_4C_1Im]I$. There is a Gaussian-shaped surface peak for $[C_4C_1Im]I$ (Figure S1a) at 2572.66 eV, with a width of 84.44 eV. Therefore, for $[C_4C_1Im]I$ we fitted a Gaussian peak plus a peak with a background function to fit the iodine sub-surface peak (Figure S1a). When fitting the iodine region for the LEIS spectra of $[C_4C_1Im]I_{1-x}[Tf_2N]_x$ where $x([Tf_2N]^-) \neq 1$, we used the $[C_4C_1Im]I$ E_F value (2573 eV) of the iodine surface peak as a constant in our fitting procedure. We also used the peak width as a constant for the iodine surface peak. As noted in the previous section here, the tail signal due to sub-surface iodine changed intensity as $x([Tf_2N]^-)$ was varied. Therefore, one needs to carefully assess whether there is an iodine surface peak present for $[C_4C_1Im]I_{1-x}[Tf_2N]_x$ where $x([Tf_2N]^-) \neq 1$. We did this by normalising the intensity of the sub-surface iodine tail signal for $x([Tf_2N]^-)$ = 0.02, 0.1, 0.2 and 0.3 (Figure S2). Clearly, the iodine regions for $x([Tf_2N]^-)$ = 0.2 and 0.3 gave the same shape (Figure S2), strongly indicating that there was no iodine surface peak for these mixtures. The iodine region for $x([Tf_2N]^-)$ = 0.1 showed a small iodine surface peak (Figure S2), and the iodine region for $x([Tf_2N]^-)$ = 0.02 showed a clear iodine surface peak (Figure S2). Therefore, for $x([Tf_2N]^-)$ = 0.3 we fitted the sub-surface background tail signal using a peak with a background function (Figure S1e). The parameters determined from this fitting were: position = 2598.072 eV, width = 135.614 eV, and shift = -10.453 eV. These parameters, along with those developed for $[C_4C_1Im]I$ (Gaussian surface peak position = 2572.66 eV, width = 84.44 eV), were used as fitting constants for $x([Tf_2N]^-)$ = 0.02, 0.1 and 0.2 (Figures S1b-d). From these fits, the area of the iodine Gaussian peak was determined for $x([Tf_2N]^-)$ = 0.02, 0.1 and 0.2.
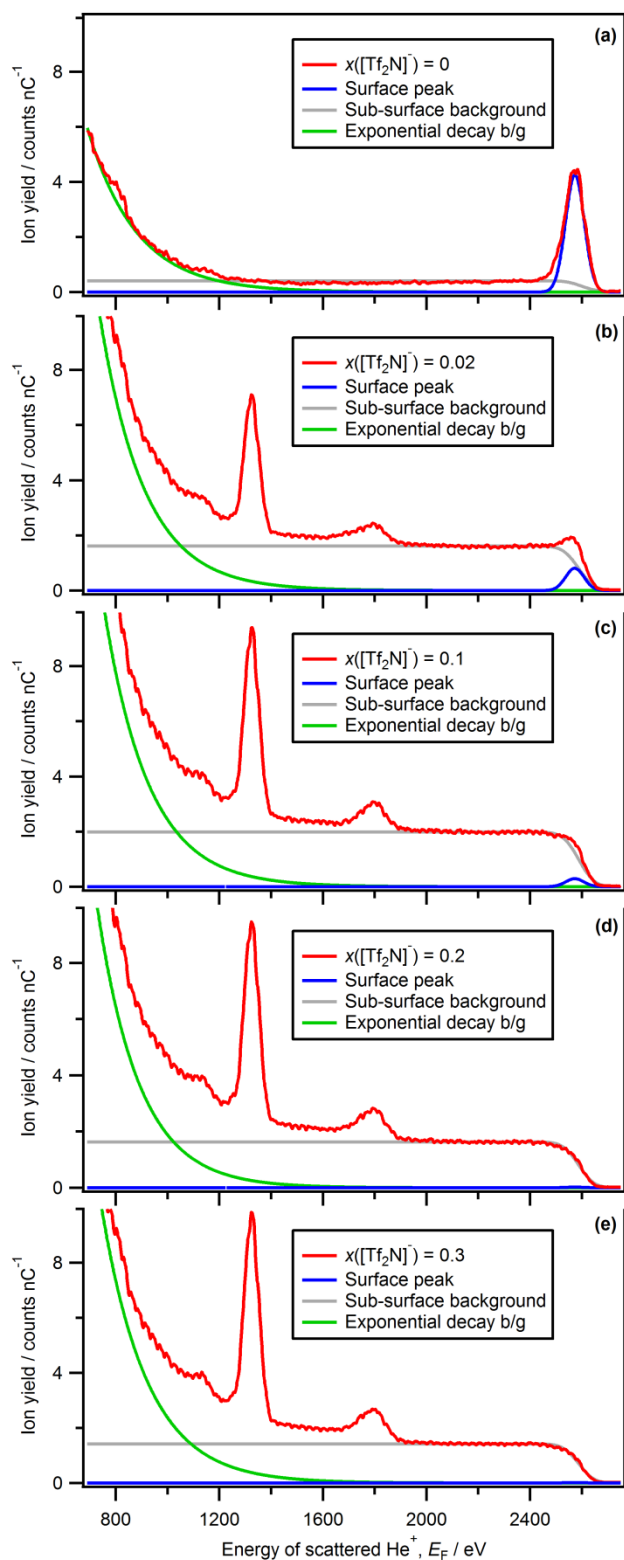
Figure S1. Fitting the iodine region of LEIS spectra (^{4}He$^+$, E_0 = 3 keV) for [C$_4$C$_1$Im]I$_{1-x}$[Tf$_2$N]$_x$: (a) [C$_4$C$_1$Im]I$_1$[Tf$_2$N]$_0$, (b) [C$_4$C$_1$Im]I$_{0.98}$[Tf$_2$N]$_{0.02}$, (c) [C$_4$C$_1$Im]I$_{0.9}$[Tf$_2$N]$_{0.1}$, (d) [C$_4$C$_1$Im]I$_{0.8}$[Tf$_2$N]$_{0.2}$, and (e) [C$_4$C$_1$Im]I$_{0.7}$[Tf$_2$N]$_{0.3}$.
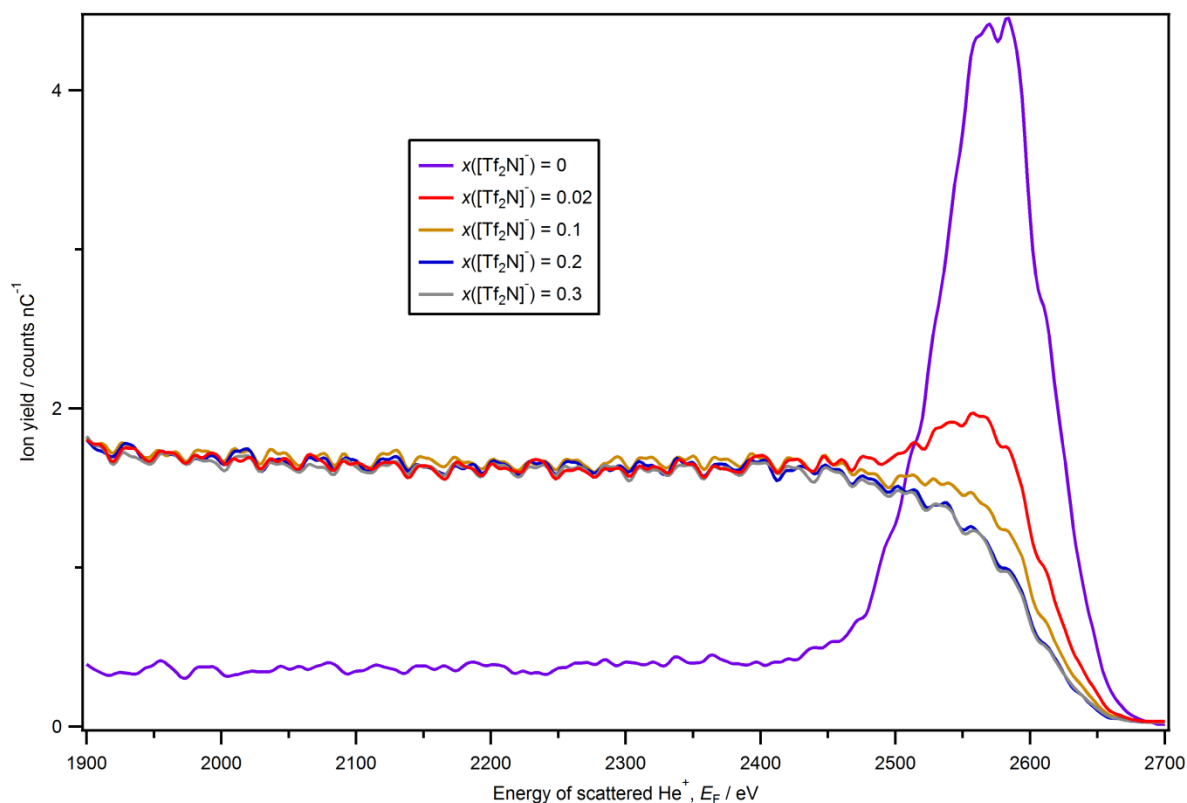
Figure S2. The iodine region of LEIS spectra (^{4}He$^+$, E_0 = 3 keV) for [C$_4$C$_1$Im]I$_{1-x}$[Tf$_2$N]$_x$. The signal intensity is normalised (apart from x([Tf$_2$N]$^-$) = 0, which is not normalised) to the signal intensity for the iodine tail signal region (~1900 eV to ~2450 eV). Iodine surface peaks can clearly be seen for x([Tf$_2$N]$^-$) = 0.02 and 0.1, but not for x([Tf$_2$N]$^-$) = 0.2 and 0.3.

9. Sample purity

A number of unexpected peaks have been observed for some of the ionic liquids studied here, which are due to contamination. By far the most commonly observed contamination peaks are due to silicon and oxygen. Silicon impurities have previously been observed using XPS for a range of ionic liquids.[22-27] The silicon and oxygen contamination is most likely from grease from synthesis of the ionic liquids. As for our previous LEIS studies on neat ionic liquids, contamination was removed by Ar$^+$ sputtering.[21]

10. Static conditions for LEIS for ionic liquids, including mixtures

It is important to demonstrate that our LEIS results are representative of the undamaged ionic liquid-vacuum surface. For mixtures in particular, it is important to investigate the equilibrium ionic liquid-vacuum surface. As the ionic liquid samples were in the LEIS chamber for at least 16 hours before LEIS experiments were carried out, we certainly expect the sample to have been at equilibrium when the LEIS experiments were begun. The 3 keV He$^+$ ions striking the outer ionic liquid surface have the potential to cause localised damage to the ionic liquid surface through both sputtering and changes in molecular structure. For our LEIS experiments, the number of He$^+$ ions that strike the ionic liquid surface during an experiment ranged from 2.0 × 10^{15} ions cm^{-2} to 1.2 × 10^{16} ions cm^{-2}; the experiments were carried over time periods ranging from 30 minutes to 120 minutes,

with an average flux of ~3.3×10^{12} ions cm^{-2} s^{-1}. These ion totals are significantly greater than the maximum recommended dose for static conditions on solid organic samples such as polymers, 10^{13} ions cm^{-2} (for metal samples the maximum recommended dose is 10^{15} ions cm^{-2}).[28] The sputter yield for our conditions is expected to be of the order of 0.1 atoms per incident He$^+$ ion, meaning the total sputter yield for an experiment is ~10^{15} atoms cm^{-2}. It has been concluded previously using XPS that ionic liquid surfaces are not significantly damaged after bombardment with Ar$^+$ ions (~1 keV).[25, 29] We have made similar observations using LEIS; clean LEIS spectra before and after Ar$^+$ bombardment are the same within the error of the experiment. Larger ions such as Ar$^+$ are expected to cause greater damage to a surface than He$^+$.[28] These observations demonstrate that any damage products produced by Ar$^+$ bombardment of the ionic liquid surface are: sputter away, vaporise away, or diffuse into bulk ionic liquid. As a typical surface is expected to contain ~5×10^{15} ions cm^{-2}, in a typical experiment, we expect that each surface atom would be struck on average once per experiment. Lísal $et\ al.$ used intrinsic analysis MD simulations to investigate the residence time for ions in [C$_n$C$_1$Im][Tf$_2$N] (n = 4, 6, 8).[18] The residence time for an ionic liquid ion in the surface layer was determined as between 0.1 ns and 1 ns.[18] Damage may occur not only at the collision site but also for surrounding ions by disrupting the surface structure. The probability of probing ionic liquid damage products at the surface of ionic liquids is minimal, as any damage products remaining in the liquid phase will diffuse away from the outer surface before another He$^+$ ion strikes that same position. Therefore, the contribution of these products to the final signal is insignificant and consequently, during our LEIS experiments we are always analysing the pristine and undamaged ionic liquid surface.
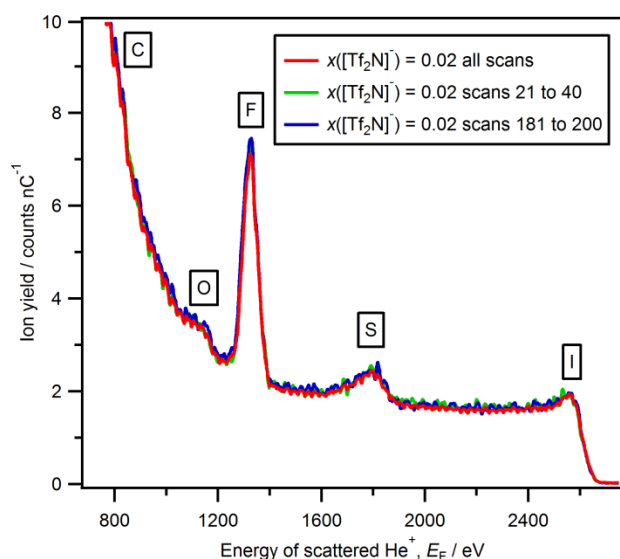

Figure S3. LEIS spectra (^{4}He$^+$, E_0 = 3 keV) for [C$_4$C$_1$Im]I$_{0.98}$[Tf$_2$N]$_{0.02}$. The three traces show all 220 scans recorded, scans 21 to 40 (recorded ~ 400 s after the start of the experiment) and scans 181 to 200 (recorded ~ 2600 s after the start of the experiment).

For neat ionic liquids, if one anion is removed by a He$^+$ collision, then another anion will readily replace it, leading to an equilibrium surface again. For mixtures, $e.g.$ [C$_4$C$_1$Im]I$_{0.98}$[Tf$_2$N]$_{0.02}$, if a [Tf$_2$N]$^-$ anion is removed by a He$^+$ collision, then to return to an equilibrium surface another [Tf$_2$N]$^-$ anion needs to replace the removed [Tf$_2$N]$^-$ anion. However, for [C$_4$C$_1$Im]I$_{0.98}$[Tf$_2$N]$_{0.02}$ the bulk [Tf$_2$N]$^-$ anion concentration is low, meaning that a replacement [Tf$_2$N]$^-$ anion will have to diffuse a larger distance

than for a neat ionic liquid. Therefore, for $[C_4C_1Im]I_{0.98}[Tf_2N]_{0.02}$ we show in Figure S3 an initial LEIS experiment (recorded ~ 400 s after the start of the experiment) and one after ~2600 s of analysis. Clearly, the two LEIS spectra are the same within the experimental error. Therefore, we can conclude for the ionic liquid mixtures the LEIS spectra were recorded for equilibrium ionic liquid-vacuum surfaces.

11. LEIS spectra for $[C_4C_1Im]Cl_{1-x}[Tf_2N]_x$
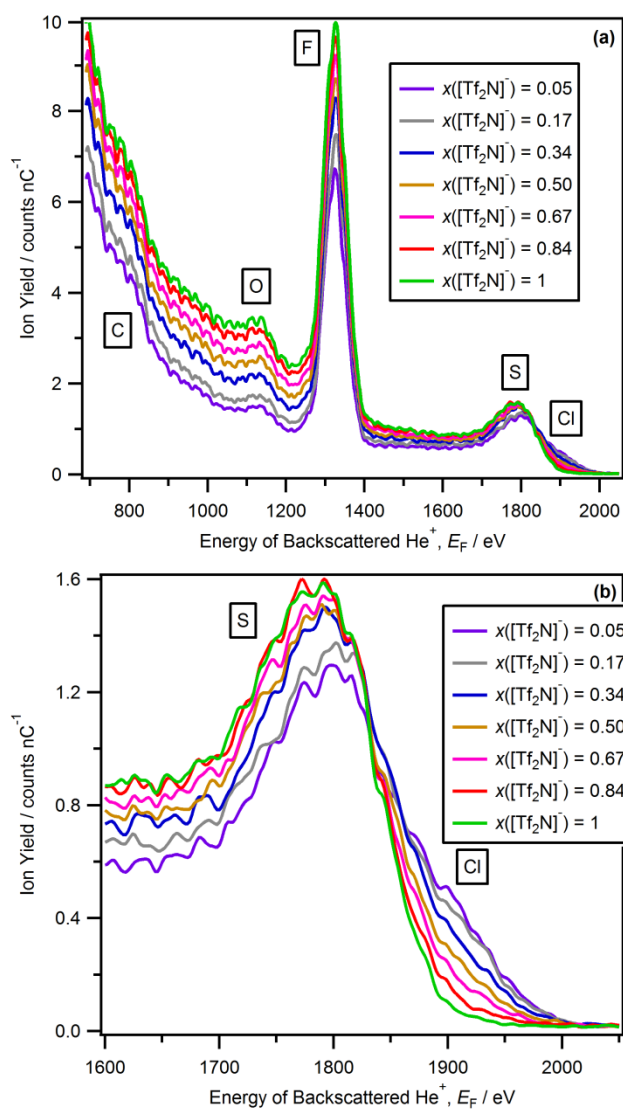
Figure S4. (a) LEIS spectra ($^4He^+$, E_0 = 3 keV) for $[C_4C_1Im]Cl_{1-x}[Tf_2N]_x$. (a) LEIS spectra ($^4He^+$, E_0 = 3 keV) for $[C_4C_1Im]Cl_{1-x}[Tf_2N]_x$ focused on E_F = 1600 eV to 2050 eV.

12. Estimating bulk amounts of each element in all ionic liquids studied: what are the ideal ionic liquid-vacuum outer atomic surfaces?

Ionic liquid	Number of each element in ionic liquid										% of each element in the bulk ionic liquid (excluding hydrogen)									
	C_{cation}	C_{anion}	N_{cation}	N_{anion}	O	S	F	B	Cl	I	C_{cation}	C_{anion}	N_{cation}	N_{anion}	O	S	F	B	Cl	I
$[C_4C_1Im][BF_4]$	8		2				4	1			53		13				27	7		
$[C_4C_1Im][Tf_2N]$	8	2	2	1	4	2	6				32	8	8	4	16	8	24			
$[C_4C_1Im][HOSO_3]$	8		2		4	1					53		13		27	7				
$[C_4C_1Im]Cl$	8		2						1		73		18						9	
$[C_4C_1Im]I$	8		2							1	73		18							9
$[C_4C_1Im]I$	8		2							1	73		18							9
$[C_4C_1Im]I_{0.98}[Tf_2N]_{0.02}$	8.00	0.04	2.00	0.02	0.08	0.04	0.12			0.98	71	0	18	0	1	0	1	0		9
$[C_4C_1Im]I_{0.9}[Tf_2N]_{0.1}$	8.00	0.20	2.00	0.10	0.40	0.20	0.60			0.90	65	2	16	1	3	2	5	0		7
$[C_4C_1Im]I_{0.8}[Tf_2N]_{0.2}$	8.00	0.40	2.00	0.20	0.80	0.40	1.20			0.80	58	3	14	1	6	3	9	0		6
$[C_4C_1Im]I_{0.7}[Tf_2N]_{0.3}$	8.00	0.60	2.00	0.30	1.20	0.60	1.80			0.70	53	4	13	2	8	4	12	0		5
$[C_4C_1Im][Tf_2N]$	8	2	2	1	4	2	6				32	8	8	4	16	8	24			
$[C_4C_1Im]Cl$	8		2						1		73		18						9	
$[C_4C_1Im]Cl_{0.95}[Tf_2N]_{0.05}$	8.00	0.10	2.00	0.05	0.20	0.10	0.30		0.95		68	1	17	0	2	1	3	0	8	
$[C_4C_1Im]Cl_{0.83}[Tf_2N]_{0.17}$	8.00	0.33	2.00	0.17	0.68	0.34	1.02		0.83		60	3	15	1	5	3	8	0	6	
$[C_4C_1Im]Cl_{0.66}[Tf_2N]_{0.34}$	8.00	0.68	2.00	0.34	1.36	0.68	2.04		0.66		51	4	13	2	9	4	13	0	4	
$[C_4C_1Im]Cl_{0.5}[Tf_2N]_{0.5}$	8.00	1.00	2.00	0.50	2.00	1.00	3.00		0.50		44	6	11	3	11	6	17	0	3	
$[C_4C_1Im]Cl_{0.33}[Tf_2N]_{0.67}$	8.00	1.33	2.00	0.67	2.68	1.34	4.02		0.33		39	7	10	3	13	7	20	0	2	
$[C_4C_1Im]Cl_{0.16}[Tf_2N]_{0.84}$	8.00	1.68	2.00	0.84	3.36	1.68	5.04		0.16		35	7	9	4	15	7	22	0	1	
$[C_4C_1Im][Tf_2N]$	8	2	2	1	4	2	6				32	8	8	4	16	8	24			
$[C_4C_1Im][HOSO_3]$	8		2		4	1					53		13		27	7				
$[C_4C_1Im][HOSO_3]_{0.98}[BF_4]_{0.02}$	8.00		2.00		3.92	0.98	0.08	0.02			53		13		26	7	1	0		
$[C_4C_1Im][HOSO_3]_{0.9}[BF_4]_{0.1}$	8.00		2.00		3.60	0.90	0.40	0.10			53		13		24	6	3	1		
$[C_4C_1Im][HOSO_3]_{0.75}[BF_4]_{0.25}$	8.00		2.00		3.00	0.75	1.00	0.25			53		13		20	5	7	2		
$[C_4C_1Im][HOSO_3]_{0.5}[BF_4]_{0.5}$	8.00		2.00		2.00	0.50	2.00	0.50			53		13		13	3	13	3		
$[C_4C_1Im][HOSO_3]_{0.24}[BF_4]_{0.76}$	8.00		2.00		1.00	0.25	3.00	0.75			53		13		7	2	20	5		
$[C_4C_1Im][BF_4]$	8		2				4	1			53		13				27	7		

Table S4. Stoichiometric amounts of each element in all ionic liquids studied.

We need a method to judge whether the changes in the LEIS spectra with x are in line with changes in the stoichiometry of the ionic liquids (*i.e.* the outer atomic surface composition matches the bulk composition, and therefore represents an ideal outer atomic surface), or whether the changes demonstrate surface structuring (*i.e.* the outer atomic surface composition is different to the bulk composition, and therefore deviates from an ideal outer atomic surface). We use the value (as %) based upon the number of each type of atom (*e.g.* $[C_4C_1Im][HOSO_3]$ contains four oxygen atoms) relative to the total number of non-hydrogen atoms (*e.g.* $[C_4C_1Im][HOSO_3]$ contains 15 non-hydrogen atoms) as a method to compare to the results from our LEIS spectra, *i.e.* the number of atoms of each element relative to the total number of non-hydrogen atoms. The results are given in Table S4.

The method we used in this article does not take into account the size of each atom. The easiest approach to account for atom size is to include the element mass in estimating the bulk amounts of each element in all ionic liquids studied. However, the differences when element mass is included is relatively small, and so we used the simplest approach, *i.e.* by simply counting the number of non-hydrogen atoms. The variations in ideal outer atomic surface composition for $[C_4C_1Im]I_{1-x}[Tf_2N]_x$ and $[C_4C_1Im]Cl_{1-x}[Tf_2N]_x$ with respect to $x([Tf_2N]^-)$ for fluorine and iodine are shown in Figures 1b and 1c respectively, and the variations in ideal outer atomic surface composition for $[C_4C_1Im][HOSO_3]_{1-x}[BF_4]_x$ with respect to $x([BF_4]^-)$ for fluorine and oxygen are shown in Figures 2b and 2c respectively. For $[C_4C_1Im]I_{1-x}[Tf_2N]_x$ and $[C_4C_1Im]Cl_{1-x}[Tf_2N]_x$ if ideal outer atomic surface compositions (an ideal surface composition matches the bulk composition) were found over the whole range of $x([Tf_2N]^-)$, then the change in the amount of anionic elements with respect to $x([Tf_2N]^-)$ would show a slight curve (Figures 1b and 1c). For $[C_4C_1Im][HOSO_3]_{1-x}[BF_4]_x$ if ideal outer atomic surface compositions were found over the whole range of $x([BF_4]^-)$, then the change in the amount of anionic elements with respect to $x([BF_4]^-)$ would be linear (Figures 2b and 2c).

13. Scattered ion yields for $[C_4C_1Im]I_{1-x}[Tf_2N]_x$ and $[C_4C_1Im][HOSO_3]_{1-x}[BF_4]_x$

The scattered ion yield for each element in each LEIS spectrum, Y_i (the area under the Gaussian peak), is proportional to the outer atomic surface concentration of each element. In the main paper (in Figures 1b, 1c, 2b and 2c) the y axes are the % surface atoms relative to simple $[C_4C_1Im][A]$ from LEIS data. Here (in Figures S5b, 5c, 6b and 6c) the y axes are Y_i from LEIS data. The % surface atoms relative to simple $[C_4C_1Im][A]$ are determined by dividing each Y_i value at x by Y_i for the simple ionic liquid (for the element of interest).

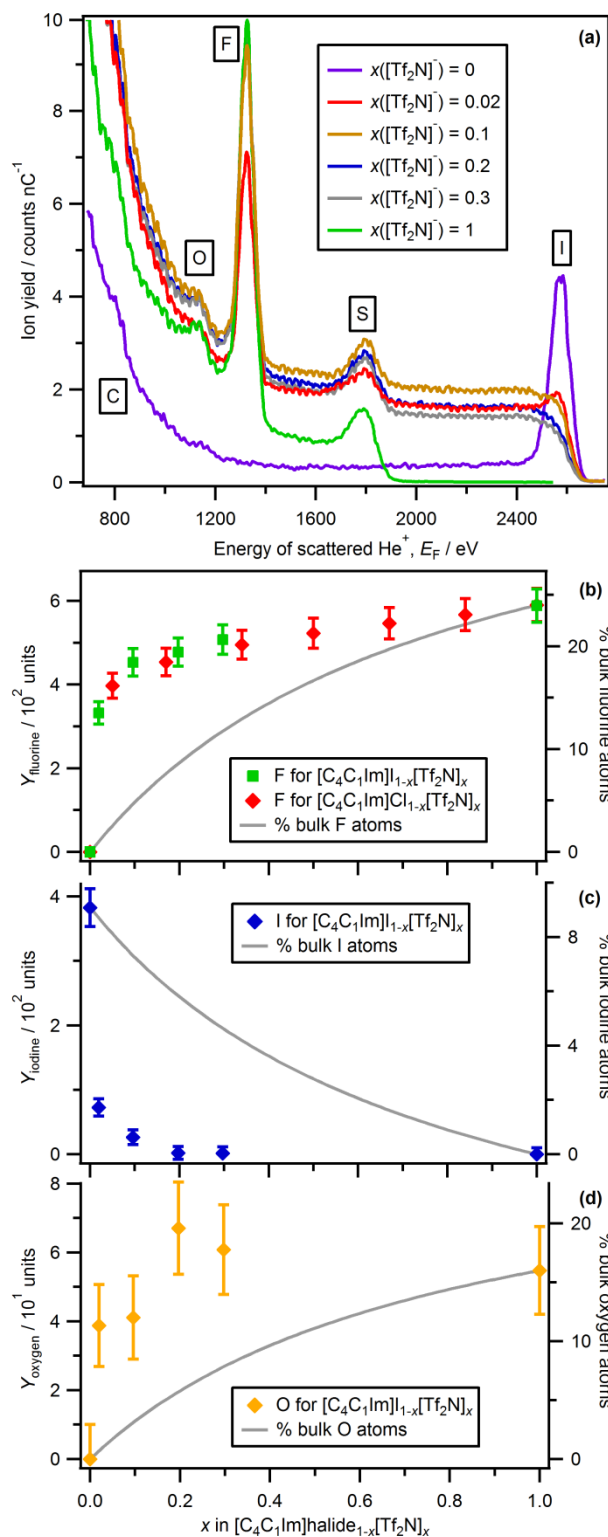**Figure S5.** (a) LEIS spectra (^{4}He$^+$, E_0 = 3 keV) for [C$_4$C$_1$Im]I$_{1-x}$[Tf$_2$N]$_x$ where x([Tf$_2$N]$^-$) = 0, 0.02, 0.1, 0.2, 0.3 and 1. (b) Ion yield for fluorine, $Y_{fluorine}$, (left axis) and % bulk fluorine atoms (which represents an ideal outer atomic surface composition, right axis) *vs*. mole fraction x([Tf$_2$N]$^-$) for [C$_4$C$_1$Im]I$_{1-x}$[Tf$_2$N]$_x$ and [C$_4$C$_1$Im]Cl$_{1-x}$[Tf$_2$N]$_x$. (c) Ion yield for iodine, Y_{iodine}, (left axis) and % bulk iodine atoms (which represents an ideal outer atomic surface composition, right axis) *vs*. mole fraction x([Tf$_2$N]$^-$) for [C$_4$C$_1$Im]I$_{1-x}$[Tf$_2$N]$_x$. (d) Ion yield for oxygen, Y_{oxygen}, (left axis) and % bulk oxygen atoms (which

represents an ideal outer atomic surface composition, right axis) *vs.* mole fraction $x([Tf_2N]^-)$ for $[C_4C_1Im]I_{1-x}[Tf_2N]_x$.
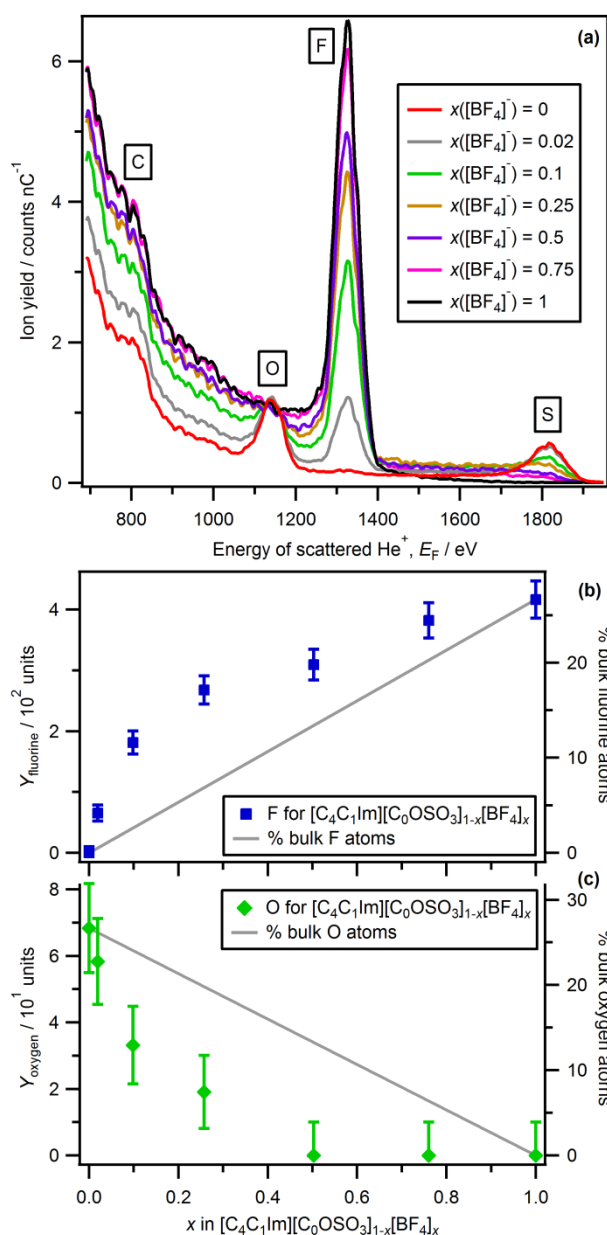
Figure S6. (a) LEIS spectra ($^4He^+$, E_0 = 3 keV) for $[C_4C_1Im][HOSO_3]_{1-x}[BF_4]_x$ where $x([BF_4]^-)$ = 0, 0.02, 0.1, 0.25, 0.5, 0.75 and 1. (b) Ion yield for fluorine, $Y_{fluorine}$, (left axis) and % bulk fluorine atoms (which represents an ideal outer atomic surface composition, right axis) *vs.* mole fraction $x([BF_4]^-)$ for $[C_4C_1Im][HOSO_3]_{1-x}[BF_4]_x$. (c) Ion yield for oxygen, Y_{oxygen}, (left axis) and % bulk oxygen atoms (which represents an ideal outer atomic surface composition, right axis) *vs.* mole fraction $x([BF_4]^-)$ for $[C_4C_1Im][HOSO_3]_{1-x}[BF_4]_x$.

14. Molecular volume, V_{mol}, and *ced* of each neat ionic liquid

- Neat $[C_4C_1Im][HOSO_3]$ and neat $[C_4C_1Im][BF_4]$ have very similar molecular volumes, V_{mol}.

- Intermolecular cation-anion interactions can be judged by the cohesive energy densities, *ced*, or the Kamlet-Taft hydrogen bond acceptor number, *β*.

	M(CA)	ρ	V_m	V_{mol}	*β*	$\Delta_{vap}H_{298}$	*ced*
Ionic liquid	g mol^{-1}	g cm^{-3}	cm^3 mol^{-1}	nm^3		kJ mol^{-1}	J cm^{-3}
[C$_4$C$_1$Im][BF$_4$]	226.1	1.19 [30]	190	0.316	0.37 [1]	152 [31]	787
[C$_4$C$_1$Im][HOSO$_3$]	236.3	1.28 [32]	185	0.308	0.67 [3]		
[C$_4$C$_1$Im][Tf$_2$N]	419.4	1.44 [30]	292	0.486	0.42 [33]	134 [34]	450
[C$_4$C$_1$Im]Cl	174.7	1.08 [2]	162	0.269	0.95 [33]	157 [35]	955
[C$_4$C$_1$Im]I	266.2	1.44 [2]	185	0.307	0.75 [33]	156 [35]	831

Table S5. *M*(CA) is the ion pair molar mass. Ionic liquid densities, ρ, to obtain ionic liquid molar volumes, V_m, and ion pair molecular volumes, V_{mol}, are taken from references [2, 30, 32]. *β* is the Kamlet-Taft hydrogen bond acceptor number; *β* from ref. [1, 3] determined using the dye set Reichardt's Dye, N,N-diethyl-4-nitroaniline and 4-nitroaniline, and *β* from ref. [33] determined using the dye set 4-tert-Butyl-2-(dicyanomethylene)-5-[4-(diethylamino)-benzylidene]-Δ3-thiazoline, 3-(4-amino-3-methylphenyl)-7-phenylbenzo-[1,2-b::4,5-b']difuran-2,6-dione and [Fe(phen)$_2$(CN)$_2$]-ClO$_4$. Therefore, as different dye sets were used, the *β* values from ref. [1, 3] and ref. [33] are not directly comparable. $\Delta_{vap}H_{298}$ are enthalpies of vaporisation at 298 K. $\Delta_{vap}H_{298}$ values for [C$_4$C$_1$Im]Cl and [C$_4$C$_1$Im]I are predicted from experimental values for [C$_8$C$_1$Im]Cl and [C$_8$C$_1$Im]I.[35] *ced* is the cohesive energy density, which is *ced* = ($\Delta_{vap}H_{298} - RT$) / V_m.

1.   M. A. Ab Rani, A. Brandt, L. Crowhurst, A. Dolan, N. H. Hassan, J. P. Hallett, P. A. Hunt, M. Lui, H. Niedermeyer, J. M. Perez-Arlandis, M. Schrems, T. Q. To, T. Welton and R. Wilding, *Phys. Chem. Chem. Phys.*, 2011, **13**, 16831-16840.
2.   J. G. Huddleston, A. E. Visser, W. M. Reichert, H. D. Willauer, G. A. Broker and R. D. Rogers, *Green Chem.*, 2001, **3**, 156-164.
3.   A. Brandt, M. J. Ray, T. Q. To, D. J. Leak, R. J. Murphy and T. Welton, *Green Chem.*, 2011, **13**, 2489-2499.
4.   H. H. Brongersma, M. Draxler, M. de Ridder and P. Bauer, *Surf. Sci. Rep.*, 2007, **62**, 63-109.
5.   H. H. Brongersma, in *Characterization of materials*, ed. E. N. Kaufmann, Wiley, Hoboken, 2nd edn., 2012, pp. 1-23.
6.   T. Cremer, C. Kolbeck, K. R. J. Lovelock, N. Paape, R. Wölfel, P. S. Schulz, P. Wasserscheid, H. Weber, J. Thar, B. Kirchner, F. Maier and H. P. Steinrück, *Chem.-Eur. J.*, 2010, **16**, 9018-9033.
7.   S. Yockel and G. C. Schatz, *J. Phys. Chem. B*, 2010, **114**, 14241-14248.
8.   J. E. Huheey, E. A. Keiter and R. L. Keiter, *Inorganic Chemistry: Principles of Structure and Reactivity*, 4th edn., HarperCollins, New York, USA, 1993.
9.   C. Waring, P. A. J. Bagot, J. M. Slattery, M. L. Costen and K. G. McKendrick, *J. Phys. Chem. Lett.*, 2010, **1**, 429-433.
10.   C. Waring, P. A. J. Bagot, J. M. Slattery, M. L. Costen and K. G. McKendrick, *J. Phys. Chem. A*, 2010, **114**, 4896-4904.
11.   B. H. Wu, J. M. Zhang, T. K. Minton, K. G. McKendrick, J. M. Slattery, S. Yockel and G. C. Schatz, *J. Phys. Chem. C*, 2010, **114**, 4015-4027.
12.   J. R. Roscioli and D. J. Nesbitt, *J. Phys. Chem. Lett.*, 2010, **1**, 674-678.
13.   J. R. Roscioli and D. J. Nesbitt, *J. Phys. Chem. A*, 2011, **115**, 9764-9773.
14.   X. H. Li, G. C. Schatz and D. J. Nesbitt, *J. Phys. Chem. B*, 2012, **116**, 3587-3602.
15.   M. P. Ziemkiewich, A. Zutz and D. J. Nesbitt, *J. Phys. Chem. C*, 2012, **116**, 14284-14294.
16.   G. Hantal, M. N. D. S. Cordeiro and M. Jorge, *Phys. Chem. Chem. Phys.*, 2011, **13**, 21230-21232.

17. G. Hantal, I. Voroshylova, M. Cordeiro and M. Jorge, *Phys. Chem. Chem. Phys.*, 2012, **14**, 5200-5213.
18. M. Lísal, Z. Posel and P. Izák, *Phys. Chem. Chem. Phys.*, 2012, **14**, 5164-5177.
19. M. Lísal and P. Izák, *J. Chem. Phys.*, 2013, **139**, 014704.
20. M. Lísal, *J. Chem. Phys.*, 2013, **139**, 214701.
21. I. J. Villar-Garcia, S. Fearn, G. F. De Gregorio, N. L. Ismail, F. J. V. Gschwend, A. J. S. McIntosh and K. R. J. Lovelock, *Chemical Science*, 2014, DOI: 10.1039/C1034SC00640B.
22. E. F. Smith, F. J. M. Rutten, I. J. Villar-Garcia, D. Briggs and P. Licence, *Langmuir*, 2006, **22**, 9386-9392.
23. K. R. J. Lovelock, E. F. Smith, A. Deyko, I. J. Villar-Garcia, P. Licence and R. G. Jones, *Chem. Commun.*, 2007, 4866-4868.
24. J. M. Gottfried, F. Maier, J. Rossa, D. Gerhard, P. S. Schulz, P. Wasserscheid and H. P. Steinrück, *Z. Phys. Chemie-Int. J. Res. Phys. Chem. Chem. Phys.*, 2006, **220**, 1439-1453.
25. C. Kolbeck, M. Killian, F. Maier, N. Paape, P. Wasserscheid and H. P. Steinrück, *Langmuir*, 2008, **24**, 9500-9507.
26. C. Kolbeck, T. Cremer, K. R. J. Lovelock, N. Paape, P. S. Schulz, P. Wasserscheid, F. Maier and H. P. Steinrück, *J. Phys. Chem. B*, 2009, **113**, 8682-8688.
27. K. R. J. Lovelock, C. Kolbeck, T. Cremer, N. Paape, P. S. Schulz, P. Wasserscheid, F. Maier and H. P. Steinrück, *J. Phys. Chem. B*, 2009, **113**, 2854-2864.
28. H. R. J. ter Veen, T. Kim, I. E. Wachs and H. H. Brongersma, *Catal. Today*, 2009, **140**, 197-201.
29. K. R. J. Lovelock, I. J. Villar-Garcia, F. Maier, H. P. Steinrück and P. Licence, *Chem. Rev.*, 2010, **110**, 5158-5190.
30. H. Jin, B. O'Hare, J. Dong, S. Arzhantsev, G. A. Baker, J. F. Wishart, A. J. Benesi and M. Maroncelli, *J. Phys. Chem. B*, 2008, **112**, 81-92.
31. A. Deyko, S. G. Hessey, P. Licence, E. A. Chernikova, V. G. Krasovskiy, L. M. Kustov and R. G. Jones, *Phys. Chem. Chem. Phys.*, 2012, **14**, 3181-3193.
32. B. Yoo, W. Afzal and J. M. Prausnitz, *J. Chem. Thermodyn.*, 2013, **57**, 178-181.
33. R. Lungwitz, V. Strehmel and S. Spange, *New J. Chem.*, 2010, **34**, 1135-1140.
34. J. P. Armstrong, C. Hurst, R. G. Jones, P. Licence, K. R. J. Lovelock, C. J. Satterley and I. J. Villar-Garcia, *Phys. Chem. Chem. Phys.*, 2007, **9**, 982-990.
35. K. R. J. Lovelock, J. P. Armstrong, P. Licence and R. G. Jones, *Phys. Chem. Chem. Phys.*, 2014, **16**, 1339-1353.